Hindawi
Advances in Materials Science and Engineering
Volume 2022, Article ID 1482877, 15 pages
https://doi.org/10.1155/2022/1482877

Review Article

Porous Silicon Formation by Electrochemical Etching

Orest Kuntyi, Galyna Zozulya, and Mariana Shepida

Department of Chemistry and Technology of Inorganic Substances, Lviv Polytechnic National University, Bandery Str. 12, Lviv 79013, Ukraine

Correspondence should be addressed to Mariana Shepida; maryana_shepida@ukr.net

Received 22 March 2022; Revised 18 April 2022; Accepted 22 April 2022; Published 27 May 2022

Academic Editor: Ştefan Ţălu

Porous silicon (PSi) is used as an effective material in biomedicine, sensors, solar cells, electrochemical energy, microelectronics, and nanotechnology. Considering the dependence of PSi functional properties on pore geometry and porous layer architecture, it is important to develop methods for controlled pore formation. After all, in the "procession" *the method of obtaining PSi ⟶ pore geometry and architecture of PSi ⟶ functional properties of PSi*, the decisive role belongs to the first participant. Among the most used methods, electrochemical etching is the most suitable for the controllability of the processes of nucleation and growth of pores since it can be controlled using the value of the current density, and the results are easily reproduced. This work analyses the literature on two types of electrochemical formation of PSi by anodic etching of (1) silicon surface and (2) silicon surface, modified with metal nanostructures. A modern explanation of the process of anodic dissolution of silicon with forming a porous surface in solutions containing HF is presented. The influence of such main factors on the process of anodic formation of PSi and its morphology is analyzed: the composition of the electrolyte and the role of each component in it; anode current density and methods of its supply (stationary, pulsed); duration; exposure to lighting; and temperature. Considerable attention is paid to the illustration of the role of alcohols and organic aprotic solvents on the formation of pore geometry. The influence of MNPs and metallic nanostructures on the process of localized metal-activated anodic etching of a semiconductor is analyzed.

1. Introduction

Porous semiconductor materials have attracted special attention during the last decade in scientific and applied aspects due to their unique physical, chemical, optical, and biological properties [1–14]. The most studied is porous silicon, which is effective in such main areas of application (Figure 1): biomedicine [6, 15], sensorics [2, 6, 15, 16], solar cells [2, 4, 8, 15], nanotechnology [2], electrochemical energetics, and microelectronics [15].

Biomedicine is the preferred choice for porous silicon due to its large surface area (200–800 $m^2 \cdot g^{-1}$) that can be loaded with drugs or bioactive species, biocompatible and biodegradable, easy sterilization. Therefore, porous silicon is considered as an effective substrate in drug delivery, tissue engineering, biomolecular screening, biosensing, etc. [1, 2, 5, 6]. A material based on PSi–porous silicon membranes is promising [13–15]. Biocompatibility, large surface area, and open-ended geometry PSiMs allow to be used in biomedical applications in such main fields: small-format hemodialysis with high toxin elimination capabilities, implantable scaffold for cell culture, scaffold for the culture of oral mucosal epithelial cells, tissue scaffold integrated with cell-laden hydrogel biomaterials, and the culture of intestinal epithelial cells.

A sensor is based on the large surface area of PSi [2], pore nanoscale [16], and synergism of 3D semiconductor substrate with metal nanostructures deposited on it [10, 17–21]. In the latter, the gain of the SERS signal is several orders of magnitude higher than on smooth silicon wafers. This provides high sensitivity for detecting amino acids, antibiotics, and amyloid proteins, which are particularly promising in biosensors.

The surface texture of PSi acts as a light trap and improves light absorption in the long-wavelength range. This allows to increase the efficiency of solar cells and reduce the cost of the material during the production of photovoltaic devices [2, 4, 8, 15, 22]. Low thermal conductivity PSi is used

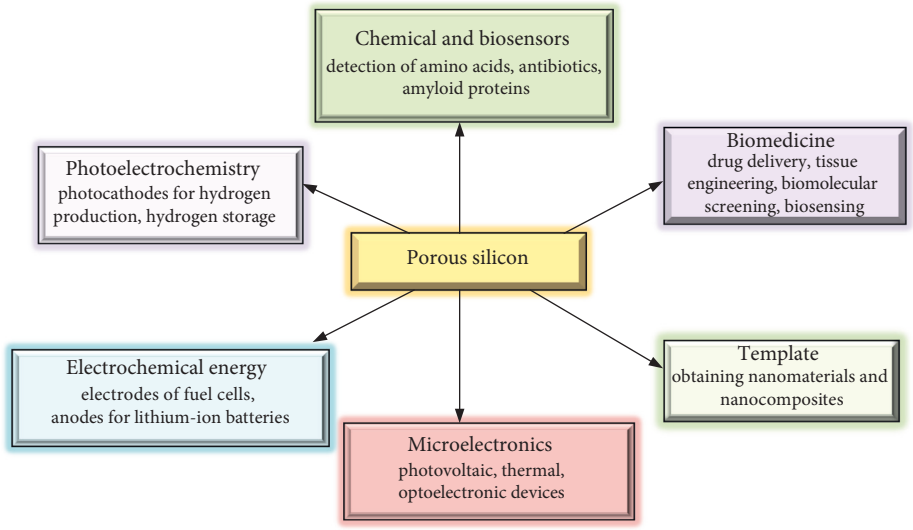

Figure 1: Applications of porous silicon.

in the manufacture of thermal devices, in particular microheaters. Applications in microelectronics include optoelectronic devices such as wavelength modulators and light-emitting capacitors [15].

Promising in electrochemical power engineering are porous silicon and silicon nanowires obtained by electrochemical etching [15, 23–25]. Thus, the authors of [23, 24] have shown the efficiency of PSi for electrodes of fuel cells, SiNWs as anodes for lithium-ion batteries [25].

The works of recent years indicate the relevance of porous silicon for photocathodes in photoelectrochemical hydrogen production [26–30] and hydrogen storage [29, 31]. Moreover, PSi and 3D silicon nanocomposite are used (PSi/PtNPs [28], PSi/(PtNPs, PdNPs) [30]).

Modern methods make it possible to obtain porous silicon of ultra-small diameter (10 nm or less) and various architecture with its high surface area and tunable pore. Due to the fact that silicon is a semiconductor, PSi has been considered in recent years as a new template for the production of nanomaterials and nanocomposites [32, 33].

The physical, physicochemical, chemical, and electrochemical methods of obtaining nanoporous silicon are known (Figure 2). The most common methods of obtaining porous silicon are stain etching [34], electrochemical etching [2–4, 10, 13–15], metal-assisted electrochemical etching [35–37], and metal-assisted chemical etching [4, 8–10].

In the "procession" *of the method of obtaining PSi ⟶ pore geometry and architecture of PSi ⟶ functional properties of PSi*, the decisive role belongs to the first participant. Thus, the choice of the method is based primarily on the controllability of the pore formation process. Electrochemical etching and metal-assisted electrochemical etching are best to meet the requirements for obtaining porous silicon with a given geometry and PSi architecture [2, 13, 22, 37]. After all, among the factors formation of pores, the main one is the value of the controlled anode current density.

Pore formation on silicon surface by electrochemical etching and metal-assisted electrochemical etching takes

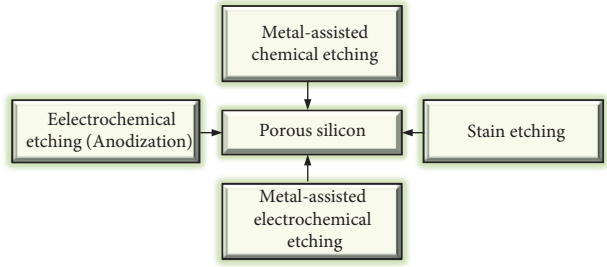

Figure 2: Methods of porous silicon obtaining.

place in fluoride-containing solutions, which is due to the nature of this semiconductor. Pore formation on the surface of silicon by electrochemical etching and metal-assisted carried out in fluoride-containing solutions [2–4, 13–15, 35–37]. This is due to the chemical nature of the semiconductor, primarily its high affinity for oxygen and a significant negative value of the standard electrode potential ($E^0_{SiO_2/Si} = -0.91$ V). Therefore, a dense water-insoluble oxide film is formed on the silicon surface in aqueous solutions at pH ≤ 7 and this oxide film dissolves in alkaline solutions (1) and HF solutions (2). Silicon also exhibits high chemical activity in such solutions (3, 4). So, electrochemical etching of silicon can be performed in two types of solutions. However, in an alkaline medium, in addition to the anodic reaction (3), a side reaction (5) is actively taking place. Therefore, in the aspect of controllability of local dissolution and minimization of the passage of side processes during the anodic formation of a porous surface, the most acceptable are fluoride-containing solutions.

$$SiO_2 + 2OH^- \longrightarrow SiO_3^{2-} + H_2O \quad (1)$$

$$SiO_2 + 6HF \longrightarrow H_2[SiF_6] + 2H_2O \quad (2)$$

$$SiO_2 + 6OH^- \longrightarrow SiO_3^{2-} + 3H_2O + 4e\left(E^0 = -1,73V\right) \quad (3)$$

$$Si + 6F^- \longrightarrow [SiF_6]^{2-} + 4e\left(E^0 = -1,2V\right) \quad (4)$$

$$Si + 2OH^- + H_2O \longrightarrow SiO_3^{2-} + H_2 \quad (5)$$

There were attempts to obtain porous silicon in a nonaqueous chloride medium, particularly organic solvents of the systems of LiCl–MeOH and LiCl–DMF solutions [38, 39]. However, anodization occurs when the values of currents are one or two orders of magnitude lower than in fluoride-containing solutions. However, anodization occurs when the values of currents are one or two orders less than in fluoride-containing solutions. In addition, the pores on the silicon surface are formed inhomogeneously. This is because ionized silicon at the anode hydrolyzes even in the presence of water traces in solutions (6), passivating the surface with an oxide film based on SiO_2. So, chloride systems are not used to obtain porous silicon.

$$Si^{4+} + 2H_2O \longrightarrow SiO_2 + 4H^+ \quad (6)$$

The process of pore formation during local anode etching of silicon in F^--containing solutions is multistage and complex. It has attracted the attention of many researchers in the last two decades [40–55]. Moreover, the electrochemical etching of the silicon surface [40–49] and Si/MNPs surface, modified with metal nanostructures [8, 50–55], has shown several differences. Therefore, they are preferably considered separately as (1) electrochemical etching method and (2) metal-assisted electrochemical etching method.

In view of the growing interest in electrochemical methods of PSi obtaining, the aim of reviews is a critical analysis of work in this area and proposals for development prospects of electrochemistry of porous silicon and intermediate products (SiNWs, SiNPs).

2. Formation of Porous Silicon by Electrochemical Etching in HF Solution

Localized etching of silicon in solutions of HF + oxidant (H_2O_2, NO_3^-, VO_2^+, Fe^{3+}) [34] by the mechanism is identical to electrochemical corrosion. It occurs due to the inhomogeneity of the surface in terms of electrode potential values. The heterogeneity is primarily due to the presence of dopants (D = B, P, Sb, As). So, anodic and cathodic areas appear on the silicon surface in the etching solution. In this case, silicon becomes a microanode, and fragments of silicon compounds with dopants (Si_xD_y) become a microcathode (Figure 3).

Electron-generating processes occur in the anode areas, which can be written by the total half-reaction (4). It leads to the local dissolution of silicon with the formation of pores. Oxidation-reduction reactions occur at the cathode areas, for example, NO_3^- to NO_2^-, VO_2^+ to VO^{2+}, Fe^{3+} to Fe^{2+}, H_2O_2 to H_2O (7), and hydrogen formation (8).

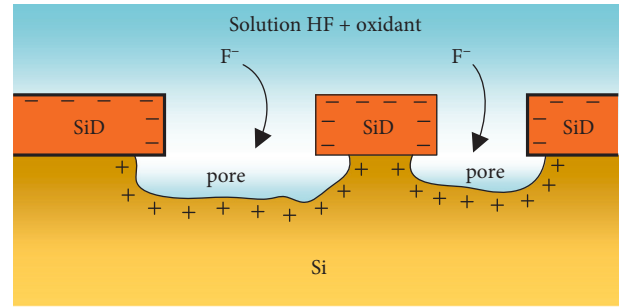

Figure 3: Scheme of silicon etching in solutions of HF + oxidant.

$$H_2O_2 + 2H^+ + 2e \longrightarrow 2H_2O \quad (7)$$

$$2H^+ + 2e \longrightarrow H_2 \quad (8)$$

A slight difference between electrode potential values (ΔE) on the surface of doped silicon between Si and Si_xD_y fragments in fluoride-containing solutions does not provide a large electromotive force and, accordingly, a high rate of the chemical etching process of a semiconductor substrate. So, this method produces only a thin layer (several microns) of porous silicon and low-aspect ratios between the pore depth and its width. So, only a thin layer (several microns) of porous silicon can be obtained by this method and low-aspect ratios between the pore depth and its width of porous silicon. In addition, chemical etching is spontaneous and does not meet modern requirements for the controllability of pore geometry and porous layer architecture. The electrochemical etching method allows to form PSi thick layers (>60 μm) with a high-aspect ratios of up to >100 (Tables 1 and 2). These advantages of ECE are due to the following. The etching of silicon atoms from the substrate takes place at applied external voltage, which leads to a shift in the potential value to more positive values. Accordingly, the density of the positive charge on the silicon surface increases. This leads to an increase in the concentration of F^- ions in the near anode layer. As a result, the rate of electrochemical (9) and chemical (10) reactions and, accordingly, the overall anodic etching process of silicon (4) increases.

$$Si + 4F^- \longrightarrow SiF_4 + 4e \quad (9)$$

$$SiF_4 + 2F^- \longrightarrow [SiF_6]^{2-} \quad (10)$$

Due to the anisotropy of doped silicon, there is local etching with the formation of pores. However, at increased i_{anode} values, the density of the positive charge on the silicon surface reaches the critical I_{EP} values (Figure 4), at which the anisotropy is levelled. That is, the difference in the surface inhomogeneity is levelled at the electrode potential values between the Si_xD_y fragments and the pure silicon fragments. This leads to uniform etching of the entire surface, i.e., its anodic polishing [2, 44, 62].

It is known that the architecture of pores and the hierarchy of the surface, as factors in the properties of porous materials, determine their main characteristics [85]. So, the controlled formation of pores geometry is a priority issue for

Table 1: Conditions for the formation of porous silicon by electrochemical etching.

Type of silicon	Electrolyte composition	Anodization parameters	Characteristics of porous silicon	Refs.
p-Si (100)	47% HF : EtOH = 2 : 1	2–40 mA·cm^{-2}, 3–180 min	Nanoporous and the macroporous layer with thickness 2–10 μm and porosity 53–58%	[56]
p-Si	47% HF:alcohol = 1 : 1,7; MeOH, EtOH, 2-PrOH, t-ButOH + SDS (surfactant)	70 mA·cm^{-2}, amplitude 14 mA·cm^{-2}, frequency 0.33 Hz, 300 s	Three layers of mesoporous silicon rugate filters with overall thickness ~ 13 μm	[57]
p-Si (100)	47%HF : H_2O:alcohol = 5 : 6 : 29 or 22 : 6 : 12; alcohol = MeOH, EtOH, PrOH, t-BuOH)	14 mA·cm^{-2}; 1 h	Macroporous structure of silicon with thickness of layers 23 μm (MeOH), 33 μm (t-BuOH)	[58]
p-Si (100)	40%HF : H_2O : EtOH = 1 : 2 : 1	140 mA·cm^{-2}, −10°C, repetition rate of 200 Hz	Porous layer with thickness 1.72–2.48 μm	[59]
n-Si (111)	40%HF : EtOH = 1 : 1	10, 30, and 50 mA·cm^{-2}, 30 min. Electrode distance 1.5, 2.0, 2.5 cm	Porous structure with pore size 0.4–0.6 μm	[60]
n-Si (100)	48%HF : EtOH = 1 : 2	10 mA·cm^{-2}, 30–60 min	Average pore size 20–1900 nm	[61]
p-Si	HF and EtOH	1–10 mA·cm^{-2}, 22°C, 5–30 min; anodization rate: 0.7–30 μm·h^{-1}	Pore size 10–110 nm; pore density: (0.03–3.3) × 10^{11} cm^{-2}; porosity: 30–78%; PSi thickness: 0.3–7.5 μm	[62]
n-Si (100)	40%HF : EtOH = 1 : 1	10–100 mA·cm^{-2} under illumination by halogen lamp; 20°C	Pore diameter: 900–1250 nm; porosity: 61–80%; pore depth: 63–69 μm	[63]
n-Si (100)	40%HF : EtOH = 1 : 3	20–100 mA·cm^{-2}, 15 min	Pore diameter: 700–1150 nm; porosity: 44–79%; pore depth: 24–36 μm	[64]
n-, p-Si (100)	HF and MeOH, EtOH or PrOH	25 mA·cm^{-2}, 20–50 min	Nanoporous silicon membrane with pore ∅ <40 nm	[65]
n-Si (100)	Low concentration of HF (5%) in H_2O and EtOH	0.47 mA·cm^{-2}, 22 min under illumination by blue LED	Thin silicon membrane with nanopore ∅ = 180 ± 12 nm	[66]
n-Si (100) n-Si (111)	HF : EtOH = 1 : 1	10–50 mA·cm^{-2}, 30 min	PSi with square pore shape on Si (100) and with the shape of the pores is a triangle on Si (111). The pores on Si (111) are distributed more evenly and more densely than those on Si (100)	[67]
n-Si (100) p-Si (100)	47% HF : EtOH] : H_2O = 1 : 2:3; 10^{-3} M CTAC	27 mA·cm^{-2}, 90 min; 40 mA·cm^{-2}, 200 min with mechanical stress	Macropore array with thickness up to 300 μm on p-Si (100)	[68]
n-Si (100)	44%HF : EtOH:37%HCl : 40% H_2O_2 : H_2O = 4 : 4:1 : 4 : 4	Pulses of peak current density: 10, 20, 50 mA·cm^{-2}; pulse duration −20 ms. 1, 2, 5 V; 15, 30, 5 min	Pore size: 50–100 nm; thickness: 54 μm; porosity PSi: 70%	[69]
n-Si (100)	48%HF, 30 wt.% H_2O_2 and EtOH in a variety of concentrations	Galvanostatic conditions. 10–300 mA·cm^{-2}; a multistep current modulation, 18 ± 1°C	Three different pore morphologies: Macro-, meso-, and micropores with 30–82% of porosities	[70]
p-Si (111)	40%HF : EtOH = 3 : 7	5–110 mA·cm^{-2}	PSi films with a branched pore geometry. Pore depth: 595–878 nm	[71]

electrochemical etching of silicon. Such a method is a multifactorial process, among which the most studied main parameters for the design of the porous structure are (1) values of anode current density; (2) composition of solution; and (3) duration of anodizing. Important parameters also include the type of silicon surface (n-, p-), which is determined by the nature of dopants and doping dose. As already mentioned (Figure 3), the latter causes electrochemical inhomogeneity of the doped silicon surface, affecting pores' initial formation. However, this issue is insufficiently studied, and individual works [13, 86, 87] do not allow to make generalizations of regularities of pore nucleation.

2.1. Influence of Anode Current Density on the Formation of Porous Silicon. Current density is the main factor of the controlling influence on the formation of porous silicon architecture. However, the nucleation and growth of pores significantly depend on the type of silicon, the HF content in the aqueous solution, the presence of alcohols and their ratio (Table 1), and the medium of organic aprotic solvents (Table 2). So, the i_{anode} value is considered in conjunction with other anodizing parameters.

Electrochemical etching is carried out mainly by stationary electrolysis [56–58, 60, 61, 63–68, 71–83]. However, attention has also been paid to nonstationary anodizing mode in recent times [59, 62, 69, 70]. But, regardless of the method of supplying current in aqueous or aqueous-alcoholic solutions and the medium of organic aprotic solvents, the anode current is the main factor that influences the electrochemical rate of reaction with the formation of SiF_4 (9). The latter forms the $[SiF_6]^{2-}$ complex anions at high concentrations of fluoride ions, according to reaction (10). The main parameter of influence on the rate of

Table 2: Conditions for the formation of porous silicon by electrochemical etching in solution with organic aprotic solvents.

Type of silicon	Electrolyte composition	Anodization parameters	Characteristics of porous silicon	Refs.
n-Si (100), n-Si (111)	2 M HF + 0.25 M TBAP in AN	7 mA·cm^{-2}, 15–60 s, 20, 30 min	Microporous structure with triangular pits	[72]
p-Si (100)	2–10 M HF + 0.1 M TBAP in DMSO, DMF or AN	2–50 mA·cm^{-2}, from 4 min to 3 h	Macropores	[73]
p-Si (100)	HF : DMF = 5 : 1; 7 : 1; 10 : 1	2–15 mA·cm^{-2}	Macropores	[74]
p-Si (100)	49% HF : DMSO:H_2O = 4 : 10 : 30	From 13 to 37 mA·cm^{-2}, 15–35°C	Macropores, porosity: 44%; SiNWs	[75]
p-Si (100)	49%HF, DMSO, and H_2O in various volume ratio	Double-step i_{anode} (11 mA·cm^{-2}, 5 min and 17 mA·cm^{-2}, 30 min), 25°C	Silicon wires with average length and ∅ 16.3 and 0.71 μm, respectively	[76]
Multicrystalline Si of p-type	HF in DMSO	Galvanostatic mode under 5 mA·cm^{-2}, 10 min	Macroporous layer. ∅≈1 μm	[77]
p-Si (100), p-Si (111)	HF and TBAP in AN, PC, or DMF; H_2O was present in the organic solutions	10–500 mA·cm^{-2}, 30 min	Macroporous layer; macropore shape p-Si (100)–round; macropore shape p-Si (111)–round or triangular; macropore ∅ = 1.0–1.6 μm; macropore depth ~9–11 μm	[78]
p-Si (100), p-Si (111)	50% HF and TBAP in AN, PC, DMF or DMSO	10 mA·cm^{-2}, 10 min	Average macropore diameter (μm)/density (μm^{-2}) in solutions: DMSO– (0.2–1.1)/ (0.6–14); DMF– (0.2–1.1)/ (0.6–14); AN– (1–1.2)/ (0.3–2); PC– (1.3)/ (0.4)	[79]
p-Si (100)	49% HF in DMF or DMSO; HF : DMF = 3 : 7; 3 : 4; HF : DMSO = 4 : 3; 3 : 4	10–300 mA·cm^{-2}, 18 ± 1°C, 16–30 μm·min^{-1}	The pore walls were very straight and smooth with the depth up to 180 μm and diameters of 1.6 μm	[80]
p-Si (100)	HF (49%):AN = 1 : 14	2.1–10.0 mA·cm^{-2}, 10 min	Pores are approximately columnar in shape with diameters of ~1 μm, extending down ~2 μm from the film surface	[81]
n-Si (100), p-Si (100)	HF (49%):DMF = 1 : 10	Galvanostatically, 2.5, 5, 7.5, 10 mA·cm^{-2}, 15, 30, 45, 60 min, using halogen or LED light	Relatively smooth cylindrical pores with ∅ = 0.1–1.3 μm, depth = 5–9 μm	[82]
p-Si (100)	HF : EtOH : DMF = 1 : 1:1	Galvanostatically, 100 mA·cm^{-2}, 5 min, 18 ± 1°C	Macroporous layer: ∅ = 1-2 μm	[83]
p-Si particles, ∅≈650 μm	10% HF in DMF	Anode etching in the barrel with ∅ = 3.5 cm, length = 3 cm, 15–100 mA, 0°C, 0.5–2 h	Thickness of the porous layer ~6.4 μm. ∅ < 100 nm	[84]

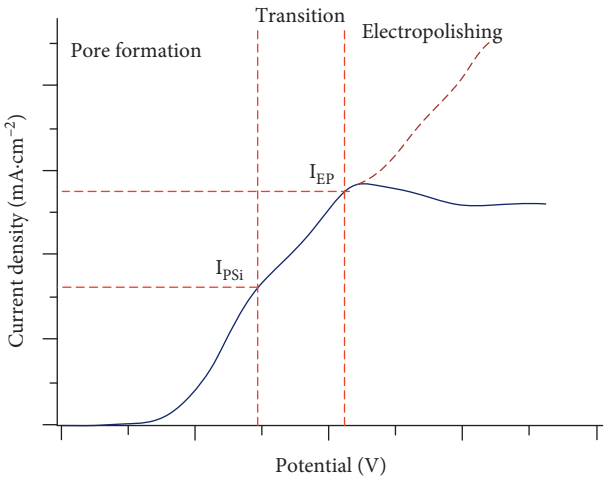

Figure 4: Stylized E-I curve of silicon anodizing in HF solutions.

electrochemical etching of silicon is i_{anode} in conditions when delivery of F^--ions is provided to the required concentration in the anodic layer and the removal of $[SiF_6]^{2-}$ complexes from it. So, with an increase in the value of anodic current density, there is a tendency to increase the pore diameter, their depth, porosity, and a change in the PSi architecture [62, 63, 67, 70, 71]. Thus, in [63], it was shown that arrays of macropores and mesopores are formed by $i_{anode} < 60$ mA·cm^{-2}, with a diameter, pore depth, and porosity of 265–760 nm, 58–63 μm, and 44–61%, respectively. At $i_{anode} > 60$ mA·cm^{-2}, the macropore arrays are formed with a diameter of 900–1250 nm, a depth of 63–69 μm, and a porosity of 61–80%. A similar effect of the anodic current on the main characteristics of PSi was observed in [67, 70]. However, this regularity is observed only in a specific range of i_{anode} values in other same conditions. After reaching the critical numbers of this value, the depth of the porous layer may decrease (Figure 5). This is primarily due to the diffuse control of reactions (9) and (10). So, in the case of F-ions "deficit" in the anodic layer, the silicon surface is passivated by reaction

$$Si + 2H_2O \longrightarrow SiO_2 + 4H^+ + 4e \quad (11)$$

Anodizing in the impulse mode of electrolysis makes it possible to accelerate diffusion processes during the pause period, which prevents the passivation of the silicon surface. It was shown in [62] that the formation rate of a porous layer

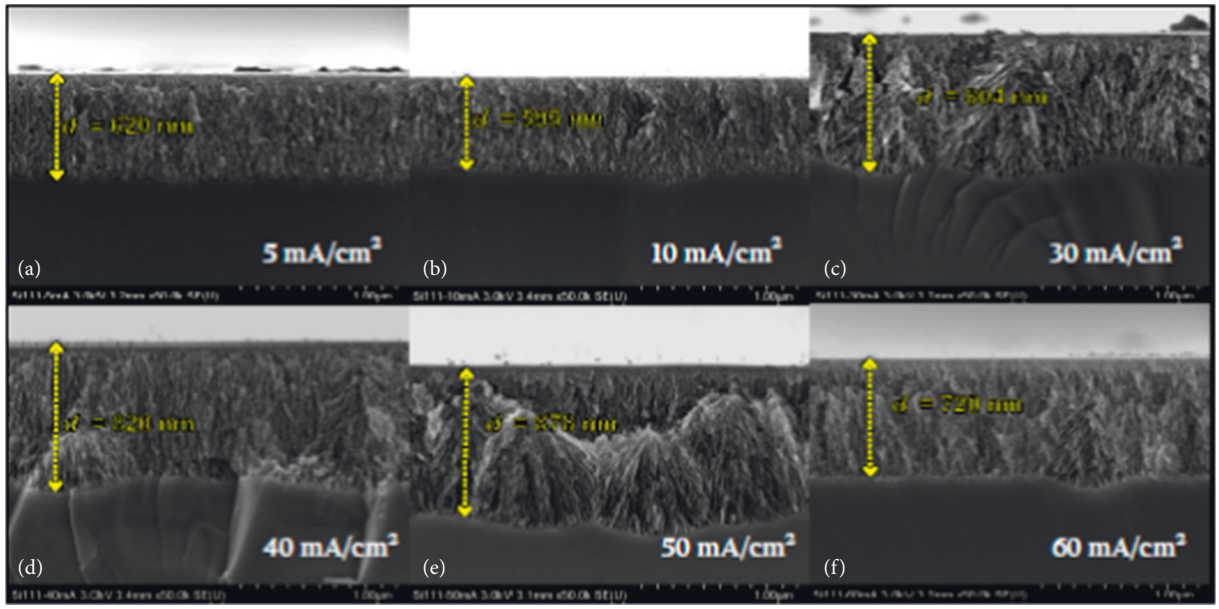

Figure 5: Cross section SEM images of PSi films at different anodizing current densities (at mA·cm^{-2}): (a) −5; (b) −10; (c) −30; (d) −40; (e) −50; (f) −60. The micrographs show the interface between the PSi film and bulk [71] under the terms of the creative commons CC BY license.

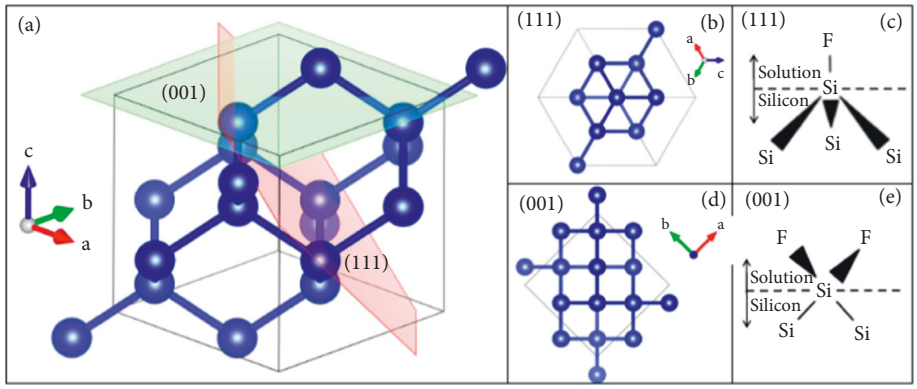

Figure 6: (a) The crystalline unit cell of silicon and the (001) and (111) planes. Crystalline cell since (b) (111) and (d) (001) planes. (c), (e) are a molecular schematic of interface solution/Si for (111) and (001) planes, respectively [71], under the terms of the creative commons CC BY license.

is two times higher at the pulse current as compared to the stationary one under the same other anodizing conditions.

By depending on pore geometry and porous layer thickness from i_{anode}, the PSi architecture can be designed. Thus, the authors of [70] showed the possibility of forming different types of bursting multilayer structures with different morphologies (macro-, meso-, and micropores) and propagation from 30 to 82% by changing the anodic current density.

The anodic density factor is not the same for silicon with different crystalline unit cell. Thus, the steric factor for F ions to Si surface atoms is more noticeable for Si (111) than for Si (001) crystalline orientation (Figure 6). So, the pore geometry is different for the same i_{anode} values (branched in Si (111) and straight in Si (001)). For Si (001), there is also a higher rate of electrochemical etching [71].

It follows from the literature analysis that the anodic current density, as an extrinsic parameter of pore formation, acts simultaneously with intrinsic parameters, which include, first of all, the nature of the doping type, doping dose, and silicon crystalline orientation. However, the effect of semiconductor crystalline orientation on pore morphology and sizes is actually limited by work [71].

2.2. Influence of Solution Composition on Anodizing Process. The main components of aqueous solutions for PSi obtained by electrochemical etching are fluoric acid and alcohols (Table 1). In a nonaqueous medium, that is, in organic aprotic solvents (Table 2), a conductive application (TBAP) is contained (in addition to HF). Each of these components performs a specific function, so their content affects the anodizing process and, accordingly, the formation of PSi.

2.2.1. Influence of Alcohols. Fluoric acid is the main reagent in electrochemical reaction (9), chemical reactions of the

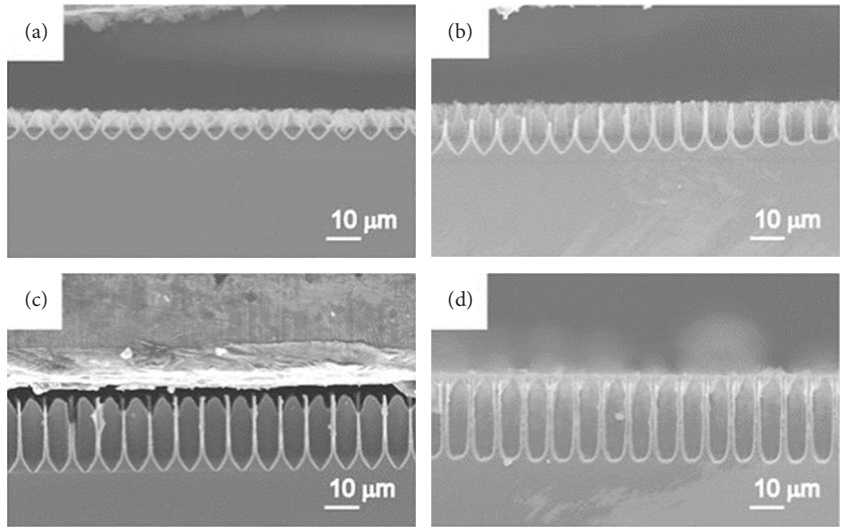

Figure 7: SEM micrographs of macropores formed in HF solutions containing various types of alcohol. Cross-sectional views of silicon anodized in a 10–20 Ωcm prepatterned p-type silicon at 14 mA·cm^{-2} for 1 h in HF solutions containing (a) MeOH, (b) EtOH, (c) PrOH, and (d) BuOH [58] under the terms of the creative commons CC BY license.

formation of the $[SiF_6]^{2-}$ complex (10), and dissolution of SiO_2 on a silicon surface (2). Therefore, HF concentration should ensure the passage of these processes at the appropriate value of i_{anode}. However, fluoric acid is also involved in a side process–the reaction with silicon, which leads to the formation of hydrogen (12). During growth, gas bubbles spontaneously create diffuse limits when they adsorb on the lateral, often rough pore surface. As a result, it is more difficult to control the formation of PSi. The alcohols are added to the anodizing solution, which limits this undesirable process (Table 1). Alcohol molecules, which adsorb on the silicon surface, lead to a decrease in the surface tension of the solution. This reduces the size of hydrogen gas bubbles and facilitates their removal from the pores. As a result, diffuse processes and, in particular, the penetration of HF are intensified. In addition, the adsorption of alcohols weakens the chemical etching of silicon, promoting the formation of a relatively smooth side surface of the pores (Figure 7).

$$Si + 6HF \longrightarrow SiF_6^{2-} + 4H^+ + H_2 + 2e \quad (12)$$

The effect of the nature of alcohols on the electrochemical etching process of silicon is little-studied. In separate works [57, 58, 65], a comparative characteristic is given of the dependence of the pores depth and their formation rate on the length of the carbon chain of the single-atom alcohol molecule. Thus, it was shown in [57] that in the series of MeOH–EtOH–PrOH–BuOH, there is a tendency to a slight increase in thickness of the porous layer, while in [58], it is focused on a significant rise of pore depth.

2.2.2. Influence of the Environment of Organic Aprotic Solvents. The study of the influence of organic aprotic solvents on the electrochemical etching of silicon began more than two decades ago using the example of an acetonitrile medium [72]. Subsequently, the electrochemical formation of porous silicon was studied in fluoride-containing solutions based on AN [73, 78, 79, 81], DMF [73, 74, 78–80, 82–84], DMSO [73, 75–77, 79, 80], and PC [78, 79]. A significant influence of organic aprotic solvents on the process of controlled anodizing of silicon with the possibility of obtaining specified pore geometries and PSi morphology is shown. However, the use of solutions of different compositions and concentrations and the difference in the modes of electrochemical etching and the difference in the types of semiconductor surface do not allow a systematic analysis of the influence of such organic solvents on the formation of porous silicon architecture (Table 2). So, we focus on the features of their action in comparison with water and alcohols. Molecules of organic aprotic solvents are characterized by a high donor number in the presence of an N- (AN) or O-donor atom (DMF, DMSO, PC). The presence of a free-electron pair and a partial negative charge promotes the formation of a hydrogen bond with the hydrogen atoms of the HF molecule, for example, $H_3C{\equiv}N{\cdots}H{-}F$, $(H_3C)_2S{=}O{\cdots}H{-}F$. This enhances the electrolytic dissociation of weak fluoric acid by shifting the equilibrium process (13) to the right, increasing the mobility of F^--ions and their diffusion permeability. In addition, the specific binding of hydrogen ions by molecules of aprotic solvent weakens its chemical activity to silicon. This prevents its etching and reduces the formation of hydrogen by reaction (12). In addition, the specific binding of hydrogen ions by molecules of aprotic solvent weakens its chemical activity to silicon, which prevents silicon etching and reduces the formation of hydrogen by reaction (12). Chemical etching of silicon, as a side process, also prevents the formation of surface complexes, for example: $H_3C{\equiv}N{:}{\longrightarrow}Si$; $(H_3C)_2S{=}O{:}{\longrightarrow}Si$. So, they perform the surfactant function, weakening side chemical processes:

$$(H_3C)_2S{=}O\ldots H-F \leftrightarrow \left[(H_3C)_2S{=}OH\right]^+ + F^- \quad (13)$$

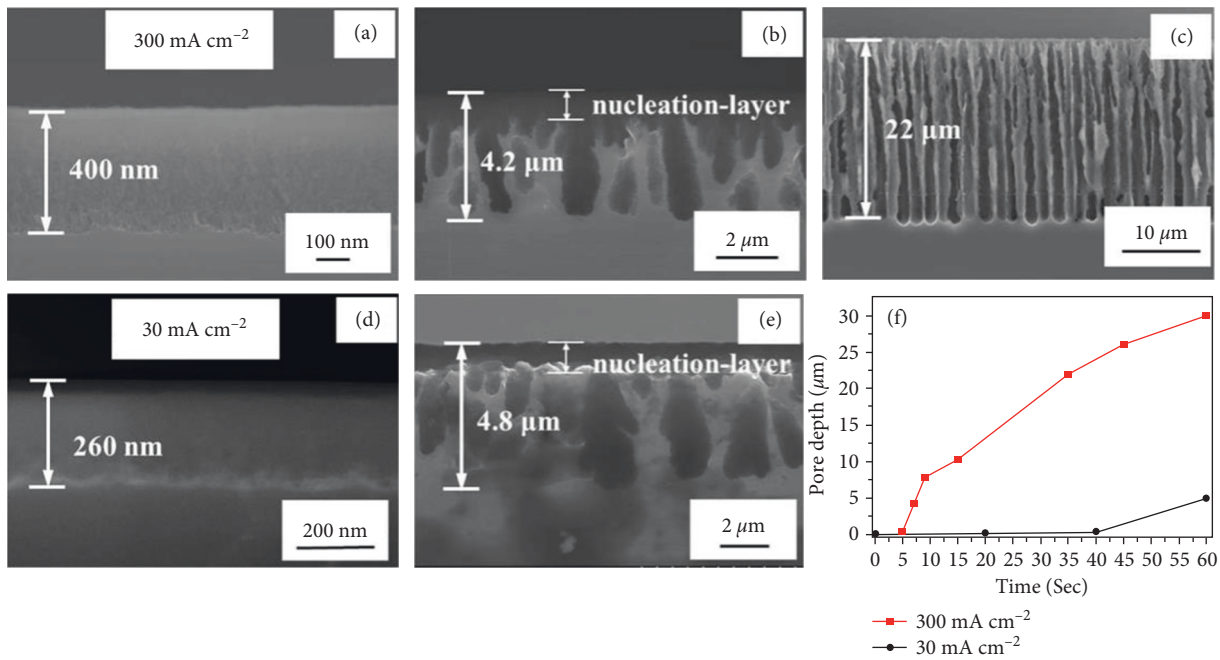

FIGURE 8: Nucleation process of p-type pore formation with different current densities: (a–c) SEM micrographs of pores formed at 300 mA·cm^{-2} over (a) 5 s, (b) 7 s, and (c) 35 s; (d, e) SEM micrographs of pores formed at 30 mA·cm^{-2} over (d) 40 s and (e) 60 s; (f) pore depth versus time. All samples were anodized in electrolyte composed of 53 vol% HF (HF : DMF = 4 : 3) [80] under the terms of the creative commons CC BY license.

The aforementioned causes the following features of the effect of organic aprotic solvents on the electrochemical etching of silicon: directional vertical formation of a predominantly smooth and cylindrical pore surface; proportional dependence of the pore depth on the i_{anode} value; obtaining a thick porous layer and a large ratio of *pore depth/diameter*; and the possibility of high rate anodizing. The formation of vertical and smooth pores was observed regardless of the nature of the organic aprotic solvent: AN [73, 78], DMF [73, 74, 78, 80, 82, 83], DMSO [73, 75–77, 80], and PC [78]. The tendency to such pore geometry is observed at the stage of nucleation and at the beginning of growth (Figures 8(a)–8(e)) and during long anodization [74, 75, 77, 78]. The work [73] shows that the pores have almost the same depth and grow parallel to each other.

After nucleation of pores, their growth in time is almost linear (Figure 8(f)). Close to linear is also the dependence of electrochemical etching rate (Figure 9), which is identical to the growth rate of the porous layer, on the i_{anode} value.

The work [80] shows the high technological prospects of dimethylformamide and dimethylsulfoxide solutions in obtaining PSi by anodizing. So, in HF–DMF and HF–DMSO, the rate of electrochemical etching reaches 16–30 μm·min^{-1} with the formation of a relatively homogeneous porous layer up to 180 μm. Moreover, the ratio of *pore depth/diameter* is controlled and very high–up to 110.

2.3. The Influence of Anodizing Duration and Energy Intensification Factors of the Porous Silicon Formation. The anodizing duration is one of parameters for the controlled PSi formation. However, this value should be considered together with other important factors, primarily the composition of the electrolyte and the anode current density. The pores geometry, the morphology of the porous layer, and the concentration of components in pores are unstable over time. This causes a change in i_{anode}, as the i_{anode} value is set on the initial area of the silicon surface. The latter increases during anodizing, so the real local i_{anode} value does not correspond to the set current density. In addition, its distribution on the porous surface is different. The concentration of fluoride ions will also be different due to diffuse restrictions caused by the inhomogeneity factor of the electric field in the pores. As a result, the dynamics of electrochemical etching of silicon changes over time. Therefore, it is advisable to consider in the tendency aspect of the dependence of the etching rate and an increase in the diameter and pores depth on the anodizing duration.

The change in the electrochemical etching rate of silicon and the pore geometry over time has not been systematically studied, which can be explained by the multifactorial nature of the anodizing process. In some works [44, 61, 62, 71, 80, 82], such dependence is fragmentarily considered as one of the characteristics of PSi formation. Thus, [44, 62, 80, 82] show a proportional increase in pore depth over a long time period. Moreover, the increase in pore depth significantly depends on the i_{anode} value (Figure 8(f)).

The energetic factors influencing the electrochemical etching process of silicon include temperature, light, and mechanical stress. Silicon anodizing is carried out mainly at room temperature (Tables 1 and 2). Higher temperatures are not used because the adsorption of alcohol molecules and organic aprotic solvents is weakened, leading to the

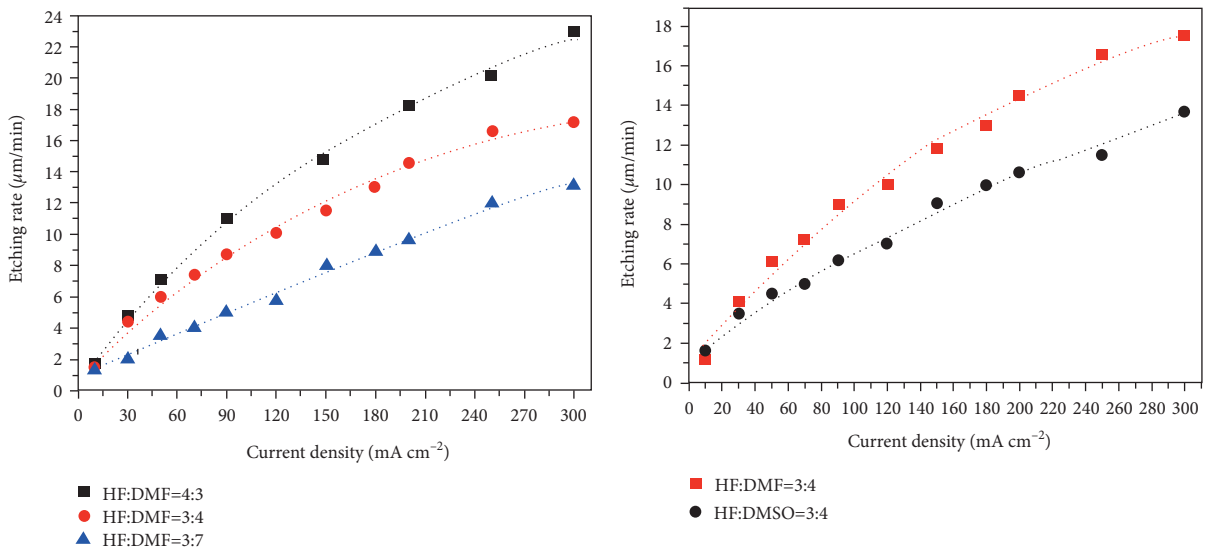

FIGURE 9: Macropore etching rate dependence on the current density in the electrolytes containing: (a) (blue triangle) HF : DMF = 3 : 7, (red spot) HF : DMF = 3 : 4, (black square) HF : DMF = 4 : 3; (b) [HF] = 43 vol% and different organic solvents: (red square) DMF; (black spot) DMSO [80] under the terms of the creative commons CC by license.

intensification of side processes, including etching with the release of hydrogen gas. As shown in [62, 84], low temperatures are effective for the formation of thick porous layers with a small pore diameter. Thus, the PSi obtained at 0°C had a pores depth of one and a half times greater and almost the same pores diameter as compared to room temperature [62].

In [40], the influence of short-wavelength light on the passage of reactions is considered, in particular, on selective and anisotropic etching, which lead to nano- and microstructuring of the silicon surface. So, illumination of silicon wafers surface is often used to design and intensify the anodizing processes at the nucleation stage and growth of a porous layer [19, 63, 66, 82]. Mechanical action, which leads to the localization of silicon surface defects by scratching [43] or mechanical stresses [68], promotes directional electrochemical etching.

3. Formation of Porous Silicon by Metal-Assisted Electrochemical Etching

One of the conditions for pores nucleation and their subsequent directed growth during chemical or electrochemical etching of a silicon surface is its electrochemical inhomogeneity. As noted earlier, such inhomogeneity is caused by alloying components, which in fluoride-containing solutions lead to the formation of anodic and cathodic regions. However, the ΔE value between them is small, which does not provide silicon's proper chemical etching rate. Therefore, electrochemical etching is more effective when its rate corresponds to the technological criteria for PSi obtaining. However, the ECE method is very sensitive to the nature of the alloying components, their content, and the orientation of the crystal lattice faces. Accordingly, the geometry of the pores and the architecture of the obtained porous layers depend on these factors. Thus, in the last decade, the method of metal-assisted electrochemical etching of silicon has attracted considerable attention (Table 3).

MAECE is a modification of the widely used metal-assisted chemical etching method of silicon [4, 8, 9, 50, 53, 91–93]. The latter method can be considered as contact electrochemical corrosion of a substrate with the Si/MNPs metals nanostructures deposited on it. Preferably M– are noble metals (Au, Ag, Pd, Pt) for which $E^0_{M^{n+}/M}{}^0 \geq 0.8$ V. This causes the high value of ΔE^0 (≥2 V) of galvanic pairs formed in fluoride-containing solutions between metal particles and silicon. Accordingly, a high rate of MACE is provided. In addition, etching is localized, and the pore geometry reproduces the shape and size of metallic nanostructures (nanoparticles and nanoporous films), which provides variety in PSi design. Metal-assisted chemical etching is carried out in similar solutions as chemical etching, i.e., HF + oxidant (mainly H_2O_2). Accordingly, the one-type processes take place - (7, 8) at the cathodic and (9, 10) at the anodic areas. At the same time, those processes' speed and etching direction significantly depend on the concentrations of fluoride and oxidant.

MAECE allows controlling the dissolution rate of silicon by changing the anodic current density. Thus, the etching direction and PSi obtaining of a given architecture is controlled [4, 36, 37, 50–55, 88–90]. Thereby, high values of i_{anode} lead to the formation of pores in a perpendicular direction to the surface, and small values—along the (100) directions [50]. In this case, silicon etching occurs at the Si/MNPs interface under the MNPs, as shown schematically in Figure 10 (left–during MACE, right–during MAECE).

During MAECE, in contrast to MACE, etching of the pores lateral surface also occurs due to anodic dissolution. As a result, conical pores are formed (Figure 11). So, comparing ECE (Figures 11(a) and 11(b)), MACE

Table 3: Metal-assisted electrochemical anodic etching conditions for the formation of porous silicon.

Type of silicon	Metal assisted	Electrolyte composition	Anodization parameters	Characteristics of porous silicon	Refs.
p-Si (100)	AgNPs	$HF : H_2O_2 : EtOH = 25 : 10 : 33$	1–40 mA·cm^{-2}, 30 min, 20°C	Sponge-like PSi layer–at low current density, mosaic layer–at high current densities	[36]
p-Si (100)	AgNPs	4.8 M HF	4 and 10 mA·cm^{-2}	SiNWs	[37]
p-Si (111), p-Si (110), n-Si (111)	AgNPs	3.6 wt % HF	0.2 mA·cm^{-2}, 90 min; 4 mA·cm^{-2}, 4 min, 20°C	Nanoporous layer. ∅ < 100 nm at 4 mA·cm^{-2} anode etching perpendicular to the surface, at 0.2 mA·cm^{-2} along <100> directions	[50]
p-Si (100), p-Si (111)	AgNPs CuNPs	3.4 wt % HF	0.2 mA·cm^{-2}, 5 mA·cm^{-2}, 20°C	Nanoporous layer. ∅ < 100 nm nanowires ∅ < 100 nm	[51]
p-Si (100)	AgNPs	$HF : H_2O_2 : EtOH = 15 : 10 : 33$; HF-40%, H_2O_2-30%, EtOH-99.7%	1, 5, 10 and 15 mA·cm^{-2}, 30 min, 20°C	Porous mosaic structure	[52]
p- c-Si	AgNPs	$HF : H_2O_2 : H_2O = 3 : 10 : 24$	5.7 mA·cm^{-2} for 60 min	Macropores layer	[53]
p-Si (100)	AgNPs	HF : DMSO:H_2O I. 2 : 5:5 II. 2 : 5:10 III. 2 : 5: 15	25°C, I. 36 mA·cm^{-2}, II. 25 mA·cm^{-2}, III. 22 mA·cm^{-2}	Ordered porous silicon and silicon wire arrays	[88]
p-Si (100)	AgNPs	$HF : H_2O_2 : EtOH = 25 : 10 : 33$; HF-40%, H_2O_2 - 30%, EtOH - 99.7%.	1 mA·cm^{-2} and 30 mA·cm^{-2}, 20°C, 30 min	Mosaic porous silicon	[89]
n-Si (100)	AgNPs AuNPs PtNPs	6.6 M HF and 0.08 M H_2O_2	20°C, 60 s photoelectrochemical etching irradiance: 17.3 mW·cm^{-2}	Mesoporous layers	[55]
n-Si (100)	Porous nanofilms of Ni, Zn, Au	$HF : EtOH = 1 : 2$	30 mA·cm^{-2}, 10 min, back illumination by halogen lamp	Columnar pores with a diameter in the range of several-hundred nanometers	[90]
p-Si (100), n-Si (100)	Nanoporous 20 nm-thick Au films	4 M HF	8 mA·cm^{-2}, 10 min; 12.5 mA·cm^{-2}, 10 min; 23 mA·cm^{-2}, 5 min; 23 mA·cm^{-2}, 5 min; 28 mA·cm^{-2}, 5 min	Si nanowires, porous Si nanowires, a porous Si layer without Si nanowires and porous Si nanowires on a thick porous Si layer	[54]

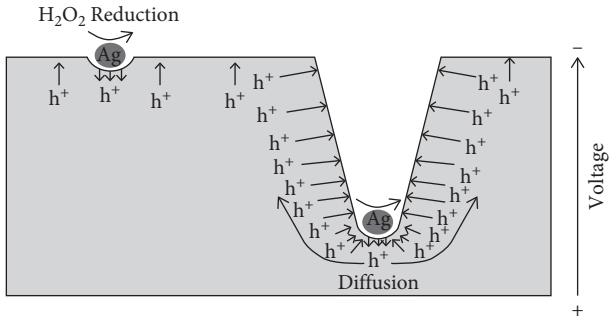

Figure 10: The model illustrates the etching mechanism of the metal–catalyzed electrochemical etching (MCECE) [53] under the terms of the creative commons CC by license.

(Figures 11(a) and 11(b)), and MAECE (Figures 11(e) and 11(f)), the authors [53] emphasize that the main difference of the latter method lies in the synergism of the activating action of the metal and the external electric field. This allows the controlled PSi formation with a wide range of pore depth and aperture size.

A feature of MAECE, in addition to the high rate of the process, is the wide design possibilities of PSi due to the geometry of deposited metal nanoparticles on a silicon surface. The nanostructured metal precipitate of the Si/MNPs system is a kind of matrix that predetermines the architecture layers. So, the main thing is to deposit MNPs of a given geometry on a silicon surface. For controlled deposition of nanostructured metals, the method of galvanic replacement [92–95], electrolysis [96–98], and sputtering [54, 90, 91, 99] are used. However, these methods do not yet provide the formation of the given geometry and topography and do not always meet the technological criteria. Yes, the galvanic replacement is technologically simple. But, the electrochemical processes that take place on the Si surface are spontaneous and multifactorial, which makes it difficult to control the deposition of nanostructured metals. Electrodeposition is characterized by effectiveness in the MNPs formation of a given geometry, but technologically it has some disadvantages—the difficulty in ensuring reliable electrical contact of the silicon surface. Sputtering requires complex and expensive equipment, which is not economically and technologically justified today.

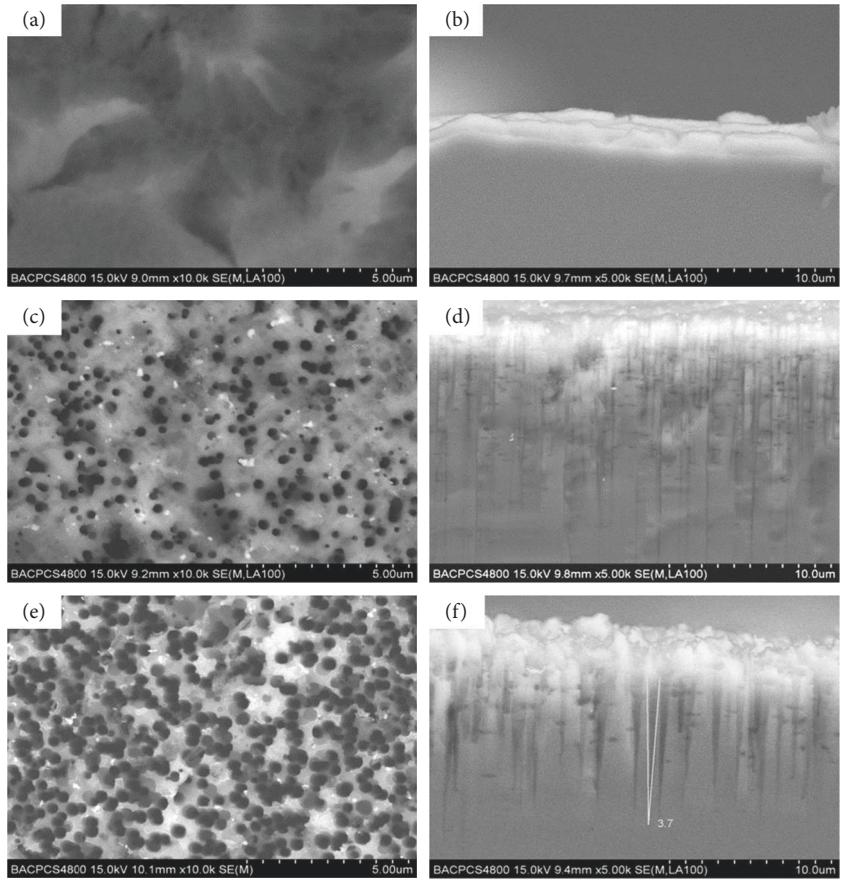

FIGURE 11: The plan and cross section SEM images of the etched c-Si surface obtained by single electrochemical etching (ECE), single metal-catalyzed electroless etching (MCEE), and metal-catalyzed electrochemical etching (MCECE) in $HF/H_2O_2/H_2O$ solution with the volume ratio of 3 : 10 : 24 for 60 min. (a) and (b): ECE with the galvanostatic condition (the current density of 5.7 mA/cm^2). (c) and (d): MCEE with the Ag particle catalyst. (e) and (f): MCECE with the galvanostatic condition (the current density of 5.7 mA/cm^2) and the Ag particle catalyst [53] under the terms of the creative commons CC by license.

4. Conclusions

Porous silicon as a semiconductor material with a large surface area and a variety of its architecture is characterized by wide functional properties, which allows its wide usage in biomedicine, sensors, solar cells, electrochemical energy, microelectronic, nanotechnology, etc. In the "cortege": *the method of obtaining PSi ⟶ pore geometry and architecture of PSi ⟶ functional properties of PSi*, the decisive role belongs to the first participant. Therefore, controlled methods of obtaining PSi are one of the priority directions in the last decade of research in this material. Electrochemical etching meets these criteria, and it is technologically promising due to the rapid production of porous silicon.

Anode etching in HF solution is based on localized PSi formation, which is due to electrochemical inhomogeneity of the silicon surface. The latter is due to the anisotropy of doped silicon or metal nanoparticles deposited on silicon. The use of such varieties for the formation of a porous layer of silicon by the methods of (1) electrochemical etching and (2) metal activated electrochemical etching is mostly described in the literature.

Porous silicon formation by electrochemical etching, which is based on the electrochemical inhomogeneity of the doped semiconductor surface, was studied in cases of aqueous solutions and organic solvents. This is a multifactorial process, and regardless of the medium, the main factors influencing the controlled formation of pore geometry and PSi architecture are the following: composition of solution; values of anode current density and methods of its supply (stationary, pulsed); and duration of anodizing, lighting, and temperature. The important parameters include the type of silicon surface, which is due to the nature of dopants, doping dose, and silicon crystalline orientation. However, representation of these issues in the literature is not enough.

The formation of porous silicon by metal-assisted electrochemical etching is a modification of the widely used and widely described in the literature metal-assisted chemical etching method of silicon. An essential feature of MAECE is that the controlling of PSi formation occurs by changing the anodic current density: high i_{anode} values lead to the formation of pores in a perpendicular direction to the surface, and small i_{anode} values—along the (100) directions. Since silicon etching occurs at the Si/MNPs interface under

the MNPs, the pore sizes and architecture of PSi are dependent on the topography of the nanostructured metal on the substrate surface. Si/MNPs are obtained mainly by the galvanic replacement method, which does not provide a fully controlled formation of MNPs in the aspect of given geometry and distribution over the surface of silicon. Thus, today this issue is one of the limiting factors for the wide practical usage of MAECE.

Abbreviations

AN: Acetonitrile
DMF: N,N-dimethylformamide
DMSO: Dimethyl sulfoxide
MeOH: Methanol
EtOH: Ethanol
n-PrOH: *n*-propanol
n-BuOH: *n*-butanol
n-PeOH: *n*-pentanol
2-PrOH: Isopropanol
t-BuOH: Tert-butanol
CTAC: Hexadecyltrimethylammonium chloride
TBAP: Tetrabutylammonium perchlorate
E: Electrode potential
GR: Galvanic replacement
i_{anode}: Anode current density
MACE: Metal-assisted chemical etching
MAECE: Metal-activated electrochemical etching
ECE: Electrochemical etching
MNCs: Metal nanoclusters
MNPs: Metal nanoparticles
NWs: Nanowires
PSi: Porous silicon
PSiMs: Porous silicon membranes
SERS: Surface-enhanced Raman scattering
SDS: Sodium dodecyl sulfate.

Data Availability

All related data are mentioned in the manuscript with references.

Conflicts of Interest

The authors declare that there are no conflicts of interest regarding the publication of this paper.

Acknowledgments

This work was carried out with the partial financial support of the National Research Foundation of Ukraine, project registration number: 2020.02/0309 ("Design of Polyfunctional Nanostructured Mono- and Bimetals with Electrocatalytic and Antimicrobial Properties").

References

[1] E. Monaico, I. Tiginyanu, and V. Ursaki, "Porous semiconductor compounds," *Semiconductor Science and Technology*, vol. 35, no. 10, Article ID 103001, 2020.

[2] E. X. Pérez, J. F. Borrull, J. Pallarés, and L. F. Marsal, "Methods, properties and applications of porous silicon," *Electrochemically Engineered Nanoporous Materials*, vol. 220, pp. 37–63, Springer Series in Materials Science, Berlin, Germany, 2015.

[3] A. Loni, "Porous silicon formation by anodization," *Handbook Of Porous Silicon*, pp. 11–22, Springer, Berlin, Germany, 2014.

[4] X. Liu, P. R. Coxon, M. Peters, B. Hoex, J. M. Cole, and D. J. Fray, "Black silicon: fabrication methods, properties and solar energy applications," *Energy & Environmental Science*, vol. 7, no. 10, pp. 3223–3263, 2014.

[5] P. A. Kulyavtsev and R. P. Spencer, "Drug delivery via porous silicon: a focused patent review," *Pharmaceutical Patent Analyst*, vol. 6, no. 2, pp. 77–85, 2017.

[6] X. Cheng and B. Guan, "Optical biosensing and bioimaging with porous silicon and silicon quantum dots (invited review)," *Progress In Electromagnetics Research*, vol. 160, pp. 103–121, 2017.

[7] S. H. Lee, J. S. Kang, and D. Kim, "A mini review: recent advances in surface modification of porous silicon," *Materials*, vol. 11, no. 12, pp. 2557–2557, 2018.

[8] M. Y. Arafat, M. A. Islam, A. W. B. Mahmood et al., "Fabrication of black silicon via metal-assisted chemical etching—a review," *Sustainability*, vol. 13, no. 19, Article ID 10766, 2021.

[9] A. A. Leonardi, M. J. L. Faro, and A. Irrera, "Silicon nanowires synthesis by metal-assisted chemical etching: a review," *Nanomaterials*, vol. 11, no. 2, pp. 383–383, 2021.

[10] N. Khinevich, H. Bandarenka, S. Zavatski et al., "Porous silicon – a versatile platform for mass-production of ultrasensitive SERS-active substrates," *Microporous and Mesoporous Materials*, vol. 323, Article ID 111204, 2021.

[11] P. H. Griffin and R. A. Oliver, "Porous nitride semiconductors reviewed," *Journal of Physics D: Applied Physics*, vol. 53, no. 38, Article ID 383002, 2020.

[12] M. Janovská, P. Sedlák, A. Kruisová, H. Seiner, M. Landa, and J. Grym, "Elastic constants of nanoporous III-V semiconductors," *Journal of Physics D: Applied Physics*, vol. 48, no. 24, Article ID 245102, 2015.

[13] N. Burham, A. A. Hamzah, and B. Y. Majlis, "Self-adjusting electrochemical etching technique for producing nanoporous silicon membrane. chapter 6 in book new research on silicon," *Structure, Properties, Technology*, IntechOpen, San Jose, CL, USA, 2017.

[14] N. Burham, A. A. Hamzah, J. Yunas, and B. Y. Majlis, "Electrochemically etched nanoporous silicon membrane for separation of biological molecules in mixture," *Journal of Micromechanics and Microengineering*, vol. 27, no. 7, 075021 pages, 2017.

[15] R. Vercauteren, G. Scheen, J. P. Raskin, and L. A. Francis, "Porous silicon membranes and their applications: recent advances," *Sensors and Actuators A: Physical*, vol. 318, Article ID 112486, 2021.

[16] S. Arshavsky-Graham, S. J. Ward, N. Massad-Ivanir, T. Scheper, S. M. Weiss, and E. Segal, "Porous silicon-based aptasensors: toward cancer protein biomarker detection," *ACS Measurement Science Au*, vol. 1, no. 2, pp. 82–94, 2021.

[17] L. A. Wali, K. K. Hasan, and A. M. Alwan, "Rapid and highly efficient detection of ultra-low concentration of penicillin G by gold nanoparticles/porous silicon SERS active substrate," *Spectrochimica Acta Part A: Molecular and Biomolecular Spectroscopy*, vol. 206, pp. 31–36, 2019.

[18] L. Mikac, M. Ivanda, V. Đerek, and M. Gotić, "Influence of mesoporous silicon preparation condition on silver clustering and SERS enhancement," *Journal of Raman Spectroscopy*, vol. 47, no. 9, pp. 1036–1041, 2016.

[19] A. M. Alwan, L. A. Wali, and M. Q. Zayer, "A new approach of pH-IEGFET sensor based on the surface modifcation of macro porous silicon with palladium nanoparticles," *Optical and Quantum Electronics*, vol. 52, p. 227, 2020.

[20] M. Škrabić, M. Kosović, M. Gotić, L. Mikac, M. Ivanda, and O. Gamulin, "Near-infrared surface-enhanced Raman scattering on silver-coated porous silicon photonic crystals," *Nanomaterials*, vol. 9, no. 3, p. 421, 2019.

[21] E. Mäkilä, A. M. Anton Willmore, H. Yu et al., "Hierarchical nanostructuring of porous silicon with electrochemical and regenerative electroless etching," *ACS Nano*, vol. 13, no. 11, pp. 13056–13064, 2019.

[22] J.-C. Lin and Y.-C. Huang, "Three-dimensional electrochemical etching by grid ditching for multi-wavelength visible-light emission on porous silicon," *Optics Express*, vol. 28, no. 22, pp. 32549–32555, 2020.

[23] M. Wang, L. Liu, and X. Wang, "A novel proton exchange membrane based on sulfo functionalized porous silicon for monolithic integrated micro direct methanol fuel cells," *Sensors and Actuators B: Chemical*, vol. 253, pp. 621–629, 2017.

[24] M. Kobayashi, T. Suzuki, and M. Hayase, "A miniature fuel cell with monolithically fabricated Si electrodes - reduction of residual porous Si on catalyst layer," *Journal of Power Sources*, vol. 267, pp. 622–628, 2014.

[25] S. Nöhren, E. Quiroga-Gonzalez, J. Carstensen, and H. Föll, "Electrochemical fabrication and characterization of silicon microwire anodes for Li ion batteries," *Journal of the Electrochemical Society*, vol. 163, no. 3, pp. A373–A379, 2016.

[26] S. Chandrasekaran, S. Vijayakumar, T. Nann, and N. H. Voelcker, "Investigation of porous silicon photocathodes for photoelectrochemical hydrogen production," *International Journal of Hydrogen Energy*, vol. 41, no. 44, pp. 19915–19920, 2016.

[27] S. Khanna, P. Marathey, S. Paneliya et al., "Fabrication of silicon nanohorns via soft lithography technique for photoelectrochemical application," *International Journal of Hydrogen Energy*, vol. 46, no. 30, pp. 16404–16413, 2021.

[28] Y. Zhao, N. C. Anderson, K. Zhu et al., "Oxidatively stable nanoporous silicon photocathodes with enhanced onset voltage for photoelectrochemical proton reduction," *Nano Letters*, vol. 15, no. 4, pp. 2517–2525, 2015.

[29] S. Chandrasekaran, T. Nann, and N. H. Voelcker, "Nanostructured silicon photoelectrodes for solar water electrolysis," *Nano Energy*, vol. 17, pp. 308–322, 2015.

[30] A. F. Halima, X. Zhang, and D. R. MacFarlane, "Photoelectrochemical characterisation on surface-inverted black silicon photocathodes by using platinum/palladium Co-catalysts for solar-to-hydrogen conversion," *Chempluschem*, vol. 83, no. 7, pp. 651–657, 2018.

[31] S. Merazga, A. Cheriet, K. M'hammedi, A. Mefoued, and N. Gabouze, "Investigation of porous silicon thin films for electrochemical hydrogen storage," *International Journal of Hydrogen Energy*, vol. 44, no. 20, pp. 9994–10002, 2019.

[32] K. Rumpf, P. Granitzer, P. Poelt, and H. Michor, "(Invited) pore filling of porous silicon with ferromagnetic nanostructures," *ECS Transactions*, vol. 69, no. 2, pp. 71–77, 2015.

[33] P. Granitzer and K. Rumpf, "Metal filled nanostructured silicon with respect to magnetic and optical properties," *Frontiers in Physics*, vol. 8, p. 121, 2020.

[34] K. W. Kolasinski, "Porous silicon formation by Stain Etching," *Handbook of Porous Silicon*, pp. 1–21, Springer, Manhattan, NY, USA, 2017.

[35] Z. Zhang, T. Martinsen, G. Liu et al., "Ultralow Broadband Reflectivity in Black Silicon via Synergy between Hierarchical Texture and Specific-Size Au Nanoparticles," *Advanced Optical Materials*, vol. 8, no. 18, Article ID 2000668, 2020.

[36] D. T. Cao, C. T. Anh, and L. T. Q. Ngan, "formation of mosaic silicon oxide structure during metal-assisted electrochemical etching of silicon at high current density," *Journal of Electronic Materials*, vol. 45, no. 5, pp. 2615–2620, 2016.

[37] D. T. Cao, C. T. Anh, and L. T. Q. Ngan, "Vertical-aligned silicon nanowire arrays with strong photoluminescence fabricated by metal-assisted electrochemical etching," *Journal of Nanoelectronics and Optoelectronics*, vol. 15, no. 1, pp. 127–135, 2020.

[38] U. L. Borkowska and J. Banaś, "Anodic dissolution of silicon monocrystals in anhydrous organic solutions of chlorides," *Electrochimica Acta*, vol. 47, no. 7, pp. 1121–1128, 2002.

[39] U. Lelek-Borkowska and J. Banaś, "Passivation and local corrosion of p-silicon in anhydrous organic solutions of chlorides. Passivation of metals and semiconductors, and properties of thin oxide layers," in *Proceedings of the A Selection of Papers from the 9th International Symposium*, pp. 245–250, Paris, France, July 2005.

[40] J. Carstensen, M. Christophersen, and H. Föll, "Pore formation mechanisms for the Si-HF system," *Materials Science and Engineering: B*, vol. 69-70, no. 70, pp. 23–28, 2000.

[41] K. W. Kolasinski, "The mechanism of Si etching in fluoride solutions," *Physical Chemistry Chemical Physics*, vol. 5, no. 6, pp. 1270–1278, 2003.

[42] K. Juodkazis, J. Juodkazytė, B. Šebeka, I. Savickaja, and S. Juodkazis, "Photoelectrochemistry of silicon in HF solution," *Journal of Solid State Electrochemistry*, vol. 17, no. 8, pp. 2269–2276, 2013.

[43] A. Slimani, A. Iratni, H. Henry et al., "Macropore formation in p-type silicon: toward the modeling of morphology," *Nanoscale Research Letters*, vol. 9, no. 1, p. 585, 2014.

[44] S. Keshavarzi, U. Mescheder, and H. Reinecke, "Formation mechanisms of self-organized needles in porous silicon based needle-like surfaces," *Journal of the Electrochemical Society*, vol. 165, no. 3, pp. E108–E114, 2018.

[45] Y. Peng, S. Jiang, Y. Tan, H. Wang, L. Wu, and L. Qian, "the formation mechanism of nondefective silicon micropatterns fabricated by scratching assisted electrochemical etching," *ECS Journal of Solid State Science and Technology*, vol. 8, no. 9, pp. P464–P471, 2019.

[46] O. Volovlikova, S. Gavrilov, D. Goroshko, E. Chusovitin, A. Pavlikov, and A. Dudin, "Formation mechanisms and photoluminescence properties of self-organized porous Si/SiO_2 structures formed by electrochemical etching of n-type of Si," *Materials Science in Semiconductor Processing*, vol. 120, Article ID 105268, 2020.

[47] I. E. Santizo and I. L. Garzón, "Geometrical model for the growth mechanism of si nanopores," *Silicon*, Springer, Manhattan, NY, USA, 2021.

[48] F. Ptashchenko, "Electrochemical etching of porous silicon – DFT modeling," *Computational Materials Science*, vol. 198, Article ID 110695, 2021.

[49] C. Y. Zhan, Y. Zou, W. Jiang et al., "Study of electrical current reconstruction on macropore arrays etched electrochemically on lightly-doped n-Si," *Applied Surface Science*, vol. 362, pp. 538–544, 2016.

[50] Z. Huang, T. Shimizu, S. Senz, Z. Zhang, N. Geyer, and U. Gösele, "Oxidation rate effect on the direction of metal-assisted chemical and electrochemical etching of silicon," *Journal of Physical Chemistry C*, vol. 114, no. 24, pp. 10683–10690, 2010.

[51] Z. P. Huang, N. Geyer, L. F. Liu, M. Y. Li, and P. Zhong, "Metal-assisted electrochemical etching of silicon," *Nanotechnology*, vol. 21, no. 46, Article ID 465301, 2010.

[52] D. T. Cao, L. T. Q. Ngan, and C. T. Anh, "Enhancement and stabilization of the photoluminescence from porous silicon prepared by Ag-assisted electrochemical etching," *Surface and Interface Analysis*, vol. 45, no. 3, pp. 762–766, 2013.

[53] Z. Li, L. Zhao, H. Diao, and H. Li, "Macroporous silicon formation on low-resistivity p-type c-Si substrate by metal-catalyzed electrochemical etching," *ECS Journal of Solid State Science and Technology*, vol. 8, no. 1, pp. 1163–1169, 2013.

[54] C. Q. Lai, W. Zheng, W. K. Choi, and C. V. Thompson, "Metal assisted anodic etching of silicon," *Nanoscale*, vol. 7, no. 25, pp. 11123–11134, 2015.

[55] A. Matsumoto, K. Iwamoto, Y. Shimada, K. Furukawa, S. Majima, and S. Yae, "Formation and dissolution of mesoporous layer during metal-particle-assisted etching of n-type silicon," *Electrochemistry*, vol. 89, no. 2, pp. 125–130, 2021.

[56] D. Hamm, T. Sakka, and Y. H. Ogata, "Porous silicon formation under constant anodization conditions: homogeneous regime or transition?" *Journal of the Electrochemical Society*, vol. 151, no. 1, pp. C32–C37, 2004.

[57] T. Urata, K. Fukami, N. Takeda, T. Sakka, and Y. H. Ogata, "Influence of solvents in HF solutions on anodic formation of mesoporous silicon, revealed by the characterization of mesoporous silicon rugate filters," *ECS Journal of Solid State Science and Technology*, vol. 5, no. 5, pp. P250–P255, 2016.

[58] T. Urata, K. Fukami, T. Sakka, and Y. H. Ogata, "Pore formation in p-type silicon in solutions containing different types of alcohol," *Nanoscale Research Letters*, vol. 7, no. 1, p. 329, 2012.

[59] L. Yongfu, "Radial microstructure and optical properties of a porous silicon layer by pulse anodic etching," *Journal of Semiconductors*, vol. 32, no. 4, 2011.

[60] R. Suryana, F. Ahmad, K. Triyana, K. Khairurrijal, and D. H. Susanto, "P. Si (111) fabrication using electrochemical anodization: effects of electrode distance and current density," *Jurnal Teori dan Aplikasi Fisika*, vol. 9, no. 1, 2021.

[61] M. Ramesh and H. S. Nagaraja, "The effect of etching time on structural properties of Porous silicon at the room temperature," *Materials Today Proceedings*, vol. 3, no. 6, pp. 2085–2090, 2016.

[62] A. M. Mebed, A. M. Abd-Elnaiem, and W. De Malsche, "Influence of anodizing parameters on the electrochemical characteristics and morphology of highly doped P-type porous silicon," *Silicon*, vol. 13, no. 3, pp. 819–829, 2021.

[63] A. Cetinel, N. Artunç, and E. Tarhan, "Influence of applied current density on the nanostructural and light emitting properties of n-type porous silicon," *International Journal of Modern Physics B*, vol. 29, no. 15, Article ID 1550093, 2015.

[64] A. Cetinel, M. Ozdogan, G. Utlu, N. Artunc, G. Sahin, and E. Tarhan, "The effect of thickness of silver thin film on structural and optical properties of porous silicon," *Surface Review and Letters*, vol. 24, no. 06, Article ID 1750074, 2017.

[65] N. Burham, A. A. Hamzah, and B. Y. Majlis, "Effects of alcohol diluents on nanopore structure of electrochemically etched silicon membrane," *Microelectronic Engineering*, vol. 141, pp. 160–167, 2015.

[66] M. S. Khan and J. D. Williams, "Fabrication of solid state nanopore in thin silicon membrane using low cost multistep chemical etching," *Materials*, vol. 8, no. 11, pp. 7389–7400, 2015.

[67] B. Pratama, I. Syahidi, E. Prayogo, K. Triyana, H. Susanto, and R. Suryana, "Formation of porous silicon on N-type Si (100) and Si (111) substrates by electrochemical anodization method," *Materials Today Proceedings*, vol. 44, no. 3, pp. 3426–3429, 2021.

[68] D. Ge, X. Huang, Z. Li et al., "Elimination of boundary effect in silicon electrochemical etching via mechanical stress," *International Journal of Materials and Structural Integrity*, vol. 10, no. 4, p. 170, 2016.

[69] M. Naddaf and R. A. Jarjour, "Free-standing porous silicon film produced by a pulsed anodic etching of n+-silicon substrate in an HF: HCl: C_2H_5OH: H_2O_2:H_2O electrolyte: characterization and adsorption of colchicine," *Silicon*, vol. 13, no. 3, pp. 739–746, 2021.

[70] D. H. Ge, M. C. Wang, W. J. Liu, S. Qin, P. L. Yan, and J. W. Jiao, "Formation of macro–meso–microporous multilayer structures," *Electrochimica Acta*, vol. 88, pp. 141–146, 2013.

[71] C. F. Ramirez-Gutierrez, I. A. Lujan-Cabrera, C. Isaza, E. K. A. Rivera, and M. E. Rodriguez-Garcia, "In situ photoacoustic study of optical properties of P-type (111) porous silicon thin films," *Nanomaterials*, vol. 11, no. 5, p. 1314, 2021.

[72] M. M. Rieger and P. A. Kohl, "Mechanism of (111) silicon etching in HF-acetonitrile," *Journal of the Electrochemical Society*, vol. 142, no. 5, pp. 1490–1495, 1995.

[73] F. A. Harraz, K. Kamada, K. Kobayashi, T. Sakka, and Y. H. Ogata, "Random macropore formation in p-type silicon in HF-containing organic solutions," *Journal of the Electrochemical Society*, vol. 152, no. 4, pp. C213–C220, 2005.

[74] J. H. Kim, K. P. Kim, H. K. Lyu, S. H. Woo, H. S. Seo, and J. H. Lee, "Three-dimensional macropore arrays in p-type silicon fabricated by electrochemical etching," *Journal of the Korean Physical Society*, vol. 55, no. 1, pp. 5–9, 2009.

[75] H. S. Jang, H.-J. Choi, H. Lee, and J. H. Kim, "Fabrication of ordered silicon wire structures via macropores without pore wall by electrochemical etching," *Journal of the Electrochemical Society*, vol. 159, no. 2, pp. D37–D45, 2011.

[76] H. S. Jang, H.-J. Choi, and S. M. Kang, "formation of p-silicon wire by electrochemical etching using positive photoresist as an etch mask in organic electrolyte," *Electrochemical and Solid-State Letters*, vol. 14, no. 8, pp. D84–D88, 2011.

[77] S. Bastide and C. Lévy-Clément, "Electrochemical macroporous texturization of multicrystalline silicon," *Journal of New Materials for Electrochemical Systems*, vol. 9, pp. 269–275, 2006.

[78] E. A. Ponomarev and C. Lévy-Clément, "Macropore formation on p-type silicon," *Journal of Porous Materials*, vol. 7, no. 1/3, pp. 51–56, 2000.

[79] S. Lust and C. Lévy-Clément, "Chemical limitations of macropore formation on medium-doped p-type silicon," *Journal of the Electrochemical Society*, vol. 149, no. 6, pp. C338–C344, 2002.

[80] D. Ge, W. Li, L. Lu et al., "Ultrafast fabrication of high-aspect-ratio macropores in P-type silicon: toward the mass production of microdevices," *Materials Research Letters*, vol. 6, no. 11, pp. 648–654, 2018.

[81] J. Peckham and G. T. Andrews, "Effect of anodization current density on pore geometry in macroporous silicon," *Semiconductor Science and Technology*, vol. 28, no. 10, Article ID 105027, 2013.

[82] J. Park, Y. Yanagida, and T. Hatsuzawa, "Fabrication of p-type porous silicon using double tank electrochemical cell with halogen and LED light sources," *Sensors and Actuators B: Chemical*, vol. 233, pp. 136–143, 2016.

[83] L. Lu, W. Li, L. Zhang, and D. Ge, "Effects of electrochemical etching conditions on the formation and photoluminescence properties of P-type porous silicon," *IOP Conference Series: Materials Science and Engineering*, vol. 484, no. 1, Article ID 012001, 2019.

[84] T. Yanagishita, S. Ueno, K. Taniguchi, and H. Masuda, "Fabrication of porous Si particles by barrel anode etching," *Chemistry Letters*, vol. 45, no. 7, pp. 708–710, 2016.

[85] S. Tălu, *Micro and Nanoscale Characterization of Three Dimensional Surfaces. Basics and Applications*, Napoca Star Publishing House, Cluj-Napoca, Romania, 2015.

[86] V. Lehmann, R. Stengl, and A. Luigart, "On the morphology and the electrochemical formation mechanism of mesoporous silicon," *Materials Science and Engineering: B*, vol. 69-70, no. 70, pp. 11–22, 2000.

[87] Y. E. Durmus, C. Roitzheim, H. Tempel et al., "Analysis on discharge behavior and performance of As- and B-doped silicon anodes in non-aqueous Si–air batteries under pulsed discharge operation," *Journal of Applied Electrochemistry*, vol. 50, no. 1, pp. 93–109, 2020.

[88] H. S. Jang, H. J. Choi, B. Y. Oh, and J. H. Kim, "Combinational approach of electrochemical etching and metal-assisted chemical etching for p-type silicon wire formation," *Electrochemical and Solid-State Letters*, vol. 14, no. 1, pp. D5–D9, 2011.

[89] D. T. Cao, C. T. Anh, and L. T. Q. Ngan, "Origin of mosaic structure obtained during the production of porous silicon with electrochemical etching," *Advanced Science, Engineering and Medicine*, vol. 11, no. 12, pp. 1218–1224, 2019.

[90] Y. Zhao, D. Li, W. Sang, D. Yang, and M. Jiang, "The optical properties of porous silicon produced by metal-assisted anodic etching," *Journal of Materials Science*, vol. 42, no. 20, pp. 8496–8500, 2007.

[91] S. Nichkalo, A. Druzhinin, A. Evtukh, O. Bratus', and O. Steblova, "Silicon nanostructures produced by modified MacEtch method for antireflective Si surface," *Nanoscale Research Letters*, vol. 12, no. 1, p. 106, 2017.

[92] O. I. Kuntyi, G. I. Zozulya, M. V. Shepida, and S. I. Nichkalo, "Deposition of nanostructured metals on the surface of silicon by galvanic replacement: a mini-review," *Voprosy Khimii i Khimicheskoi Tekhnologii*, vol. 3, pp. 74–82, 2019.

[93] M. Shepida, O. Kuntyi, S. Nichkalo, G. Zozulya, and S. Korniy, "Deposition of gold nanoparticles via galvanic replacement in DMSO and their influence on formation of silicon nanostructures," *Advances in Materials Science and Engineering*, pp. 1–7, Article ID 2629464, 2019.

[94] M. Tran, S. Roy, S. Kmiec et al., "formation of size and density controlled nanostructures by galvanic displacement," *Nanomaterials*, vol. 10, no. 4, 644 pages, 2020.

[95] M. Shepida, O. Kuntyi, G. Zozulya, and E. Kaniukov, "Deposition of palladium nanoparticles on the silicon surface via galvanic replacement in DMSO," *Applied Nanoscience*, vol. 10, no. 8, pp. 2563–2568, 2020.

[96] F. Lima, U. Mescheder, C. Müller, and H. Reinecke, "Copper electrodeposition on silicon electrodes," *International Journal of Surface Science and Engineering*, vol. 12, no. 2, pp. 99–118, 2018.

[97] M. V. Shepida, O. I. Kuntyi, O. Y. Dobrovets'ka, S. A. Kornii, and Y. I. Eliyashevs'kyi, "Deposition of gold nanoparticles on silicon in the pulse mode of electrolysis in a DMSO solution," *Materials Science*, vol. 55, no. 3, pp. 417–423, 2019.

[98] O. Kuntyi, M. Shepida, O. Dobrovetska, S. Nichkalo, S. Korniy, and Y. Eliyashevskyy, "Pulse electrodeposition of palladium nanoparticles onto silicon in DMSO," *Journal of Chemistry*, vol. 2019, Article ID 5859204, 8 pages, 2019.

[99] Y. Zhao, D. Li, and D. Yang, "Al-assisted anodic etched porous silicon," *Journal of Materials Science*, vol. 41, no. 16, pp. 5283–5286, 2006.